Can we retrieve information from quantum thermalized states?

C. M. Lóbez[1] **and A. Relaño**[1]

[1] Departamento de Estructura de la Materia, Física Térmica y Electrónica, and GISC Universidad Complutense de Madrid, Av. Complutense s/n 28040, Madrid, Spain

Abstract.

We propose a protocol to prepare thermalized states storing relevant amounts of information about their past, and we study their resilience and the conditions under which we can profit from them. This protocol is based on the existence of an integrable stage in the preparation process, which makes it possible to record these amounts of information in the expected value of the corresponding integral of motion. By means of numerical calculations on the paradigmatic Dicke model, we show that it is possible to lead a quantum system onto a highly chaotic region, in which the eigenstate thermalization hypothesis is fulfilled and hence we find thermalization, without erasing this information. Notwithstanding, we also propose the existence of a quantum mechanism that mimics the high sensitivity to initial conditions trademark of classical chaos, and thus constitutes a powerful tool for information erasure. Its efficiency is rapidly increased with the number of particles, and hence the proposed protocol is only applicable to small quantum systems. It is induced by avoided level crossings in the transition from integrability to chaos, and it is switched on when the system goes through this transition with finite rapidity. We also show that the same mechanism contributes to hide this information from equilibrium measurements when the system follows the same path in the adiabatic limit.

Keywords: Quantum thermalization, Connections between chaos and statistical physics.

1. Introduction

We are used to assuming that thermal equilibrium is due to the effective erasure of all the information about previous conditions of the system. This is what happens in classical statistical mechanics. Due to chaos and ergodicity, any trajectory samples the whole available region of the phase space; and because of extreme sensitivity to initial conditions, it becomes impossible to trace back its past, and even to demarcate a region in which the initial state was likely to be. In such circumstances, the expected values of observables in isolated classical systems are well described by microcanonical averages,

$$\langle \mathcal{O} \rangle = \lim_{\tau\to\infty} \frac{1}{\tau} \int_0^\tau dt\, \mathcal{O}(p[t], q[t]) = \frac{\int_{\mathcal{M}} dpdq\, \mathcal{O}(p,q)\delta[E - H(p,q)]}{\int_{\mathcal{M}} dpdq\, \delta[E - H(p,q)]}, \tag{1}$$

where $H(p,q)$ is the Hamiltonian, (p,q) represents all the momenta and coordinates of the system, and $\mathcal{M}$ indicates that the integration is done over the complete phase space.

The scenario is completely different in the quantum realm. The wavefunction of any isolated quantum system evolves as

$$|\psi(t)\rangle = \sum_j c_j(0) \exp(-iE_j t/\hbar)\, |E_j\rangle\,, \tag{2}$$

where $\{|E_j\rangle\}$ are the eigenstates of the Hamiltonian, and $c_j(0) = \langle E_j|\psi(0)\rangle \equiv c_j$ represent the initial condition. The expectation value of any quantum observable $\hat{O}$ in this state is:

$$\langle\psi(t)|\, \hat{O}\, |\psi(t)\rangle = \sum_j |c_j|^2 \langle E_j|\, \hat{O}\, |E_j\rangle + \sum_{i\neq j} c_i^* c_j \mathsf{e}^{-i(E_j - E_i)t/\hbar} \langle E_i|\, \hat{O}\, |E_j\rangle\,. \tag{3}$$

And therefore its long-time average is equal to:

$$\left\langle \hat{O} \right\rangle = \lim_{\tau\to\infty} \frac{1}{\tau} \int_0^\tau dt\, \langle\psi(t)|\, \hat{O}\, |\psi(t)\rangle = \sum_j |c_j|^2 \langle E_j|\, \hat{O}\, |E_j\rangle\,, \tag{4}$$

if the spectrum has no degeneracies, that is, if $E_i \neq E_j$, $\forall\, i \neq j$.

Even though both Eqs. (1) and (4) apply to isolated systems, in which the energy, E, is constant, there are significant differences between them. The first one is correct only in strongly chaotic —ergodic and mixing— classical systems, and its only relevant parameter is the conserved energy, E. The second one is valid for any isolated quantum system (with no degeneracies in the sequence of energy levels), and depends on all the coefficents $|c_j|^2 = |\langle E_j|\psi(0)\rangle|^2$, that is, on a very large, maybe infinite, set of numbers linked to the initial condition. Hence, although Eq. (4) constitutes an effective equilibrium state, around which the system stays most of the time [1, 2], it seems to contradict the first sentence of this paper. To reach this quantum equilibrium state, the time evolution has erased the relative phases between the coefficents $c_j = \langle E_j|\psi(0)\rangle$ —this process is usually called *dephasing* [3]—, but it keeps all the information stored in a very large set of numbers, $|c_j|^2$.

Notwithstanding, it is well known that the information stored in the coefficents $|c_j|^2$ is not necessary to account for the expected values of relevant observables under many

circumstances. On the contrary, a microcanonical average,

$$\left\langle \hat{O}(E) \right\rangle_{ME} = \frac{1}{\mathcal{N}} \sum_{E' \in [E, E+\Delta E]} \langle E' | \hat{O} | E' \rangle , \tag{5}$$

where $\mathcal{N}$ is the number of energy eigenstates inside a small energy window, ΔE, provides a good description for physical observables in quantum chaotic systems [4].

The equivalence between Eqs. (4) and (5) is sustained by the Eigenstate Thermalization Hypothesis (ETH), which is expected to hold in chaotic quantum systems [3, 5, 6, 7, 8, 9]. This hypothesis does not refer to how the time evolution erases the information stored in the initial condition, but to the shape of the matrix elements $\langle E_n | \hat{O} | E_n \rangle$ present in Eq. (4). In particular, the ETH establishes that in thermalizing systems, that is, in quantum isolated systems for which the microcanonical average, Eq. (5), provides a good description, the matrix elements of physical observables in the basis of Hamiltonian eigenstates read

$$\langle E_m | \hat{O} | E_n \rangle = O(\overline{E}) \delta_{nm} + \mathrm{e}^{-S(E)/2} f_O(\overline{E}, \omega) R_{nm}, \tag{6}$$

where $\overline{E} = (E_m + E_n)/2$ and $\omega = E_m - E_n$. $O(\overline{E})$ and $f_O(\overline{E}, \omega)$ are smooth functions; in particular $O(\overline{E})$ is expected to be equal to the microcanonical average, $\left\langle \hat{O}(E) \right\rangle_{ME}$. $S(\overline{E})$ is the thermodynamic entropy, and R_{nm} is a random variable with zero mean and unit variance. Applied to the diagonal elements present in Eq. (4), $\langle E_n | \hat{O} | E_n \rangle$, Eq. (6) establishes that

$$\langle E_n | \hat{O} | E_n \rangle = \left\langle \hat{O}(E) \right\rangle_{ME} + \Delta_n, \tag{7}$$

where E can be understood as a macroscopic coarse-grained energy, and Δ_n is a random noise whose width decreases fast with the system size. In its stronger version, the ETH establishes that all the values of Δ_n become negligible in the thermodynamic limit; for its weaker version, it suffices that most Δ_n fulfill this condition [10, 11].

Due to the difficulty in performing exact calculations in large quantum systems, it is not clear whether the strong version of the ETH is necessary, or it is enough to fulfill its weaker version. Furthermore, it has been recently shown that the presence of correlations in the sequence of Δ_n increases the probability of finding atypical non-thermalizing initial conditions [12, 13]. Anyhow, the most important consequence of the ETH becomes visible if Eq. (7) is introduced in the expression for the exact time average of observables, Eq. (4),

$$\left\langle \hat{O} \right\rangle = \sum_j |c_j|^2 \langle E_j | \hat{O} | E_j \rangle = \sum_j |c_j|^2 \left\langle \hat{O}(E_j) \right\rangle_{ME} + \sum_j |c_j|^2 \Delta_j. \tag{8}$$

As the argument in $\left\langle \hat{O}(E) \right\rangle_{ME}$ is not a microscopic, but a macroscopic coarse-grained energy, we can approximate the former expression to:

$$\left\langle \hat{O} \right\rangle \approx \left\langle \hat{O}(E) \right\rangle_{ME} + \sum_j |c_j|^2 \Delta_j, \tag{9}$$

if the distribution of coefficents $|c_j|^2$ is narrow enough to make $|c_j|^2 \neq 0$ only within a window with macroscopically negligible width. This expression shows that, if ETH

is fulfilled and thus the fluctuations Δ_n are negligible, *the information stored in the coefficents* $|c_j|^2$ *is not relevant for the expected values of physical observables.* This implies that the mechanisms of thermalization are totally different in the classical and the quantum realms. Clasically, the information stored in the initial condition is erased by chaos; in the quantum realm, this information might be still present, but it would be irrelevant for the expected values of observables in equilibrium. In other words, the fact that quantum equilibrium values coincide with microcanonical averages is not enough to infer that these states have no information about their past —the ETH just hampers the possibility of reading such information by means of equilibrium measurements.

The ETH can be thus understood as a sufficent condition for thermalization. Notwithstanding, it is important to emphasize that it is not necessary. On the contrary, it is possible to obtain thermalization in systems in which the conditions for the ETH do not hold [14]. For example, let us imagine that we prepare a quantum state in which the distribution of coefficents $|c_j|^2$ is narrow and smooth. Then, it is straightforward to see that

$$\sum_j |c_j|^2 \langle E_j| \hat{O} |E_j\rangle \simeq \left\langle \hat{O}(E) \right\rangle_{ME}, \tag{10}$$

independently of the values of $\langle E_j| \hat{O} |E_j\rangle$. In such a case, the mechanisms for classical and quantum thermalization are very similar. However, as the distribution of coefficents $|c_j|^2$ depends on the initial condition, it seems possible to design preparation protocols in which this scenario does not hold.

In this paper, we propose a protocol to prepare thermalized states storing relevant amounts of information about their past, and we show that this information can be tracked by means of adequate measurements. Its key element is the existence of an intermediate integrable stage in the preparation process. However, we unveil that this information is quite fragile. The transition from integrability to chaos is accompanied by an efficent mechanism of information erasure, induced by avoided level crossings, that enhances the sensitivity to initial conditions. Furthermore, we show that the same mechanism *hides* the information which is still stored in the coefficents $|c_j|^2$ when the protocol is performed adiabatically, so that we cannot read it by means of equilibrium measurements, even within an integrable region. A remarkable fact is that the mechanism of information erasure is the consequence of changing the system Hamiltonian fast enough, and therefore can be overcome if such changes are slowed down. In contrast, the extreme sensitivity to initial conditions, trademark of classical chaos, implies that the corresponding information erasure cannot be avoided, and therefore the main results of this paper cannot be reproduced in a classical numerical experiment. We note here that the problem of recovering quantum information under different circumstances is object of current research, for example when a quantum measurement damages a time-reversed protocol [15, 16].

The paper is organized as follows. In Section 2 we introduce all our numerical tools, including the model we work with. In Section 3 we perform a first set of numerical experiments, showing that we can prepare thermalized states storing relevant pieces

of information about their past within a highly chaotic region. We also discuss how this information can be recovered. In Section 4 we perform another set of numerical experiments to study the mechanisms of information erasure. Finally, in Section 5 we briefly discuss all these results.

2. Numerical tools and notation

2.1. The Dicke model

All the numerical experiments discussed in this work are based on the Dicke model. It was introduced in 1954 by R. H. Dicke [17], and is the object of current experimental research [18, 19, 20, 21, 22, 23]. It describes the interaction of N two-level atoms of splitting ω_0 with a single bosonic mode of frequency ω. Its Hamiltonian reads

$$\mathcal{H} = \omega_0 J_z + \omega a^\dagger a + \frac{2\lambda}{\sqrt{N}} J_x (a^\dagger + a), \tag{11}$$

where λ is the coupling constant, a and $a^\dagger$ are the usual anihilation and creation operators for the bosonic field, and $\vec{J}$ is an angular momentum accounting for the collective atomic dynamics. As $[H, J^2] = 0$, we restrict ourselves to $j = N/2$, which deals with the recent experimental realizations [18, 19, 20, 21, 22, 23]. The parity $\Pi = \exp(i\pi[j + J_z + a^\dagger a])$ also commutes with the Hamiltonian.

The rich phenomenology of this model provides an excellent framework to study thermalization and information storage in isolated quantum systems. First of all, it has thermal [24, 25, 26], quantum [27, 28] and excited-state quantum phase transitions [29, 30, 31, 32]. Hence, the Dicke model is an excellent test model to study how thermalization is affected by a phase change. For our purposes, it is even more interesting that it exhibits a crossover from integrability to chaos, in terms of the coupling constant, λ, the ratio of atomic and photonic frequencies, ω_0/ω, and the energy, E. It has an approximate integral of motion,

$$J'_z = \frac{J_z + \sqrt{\frac{4\lambda^2}{\omega_0 N}} \left(a + a^\dagger\right) J_x}{\sqrt{1 + \frac{4\lambda^2}{\omega_0 N} \left(a + a^\dagger\right)^2}}, \tag{12}$$

valid in the low-energy region of the strong coupling regime, $\lambda > \sqrt{\omega\omega_0}/2$ [33, 34]. Within this region, the energy spectrum is very approximately divided in bands labelled by an extra quantum number $m' = -j, -j+1, \ldots, j$, given by the corresponding value of $\langle J'_z \rangle$; the larger the coupling λ and the ratio ω_0/ω, and the smaller the energy, the better this aproximation. The transition to chaos happens when this integral of motion ceases to exist. Detailed analysis of this crossover from integrability to chaos and its consequences can be found in [35, 36, 37].

The Dicke model has also a classical version which provides a good description of its thermodynamic limit, $N \to \infty$; it is possible to define an effective Plack constant, $\hbar_{\text{eff}} = 2/N$ [38]. This limit makes it possible to perform a direct comparison between classical and quantum dynamics. As a consequence, it has been recently shown that

classical Lyapunov exponents, trademark of chaos, also play a very important role in the scrambling of quantum information [39, 40].

Throughout this paper we consider $\omega = \omega_0 = \hbar = 1$. With this choice, both the quantum and the classical versions of the Dicke model are strongly chaotic if $\lambda > 1/2$ and $E/j > -1$ [33, 34, 36].

2.2. Numerical protocols

The aim of this paper is to study the information encoded in different equilibrium states of the quantum version of the Dicke model. To do so, we track the time evolution of particular initial states, keeping the system thermally isolated. All our numerical experiments rely on changing the coupling constant of the Dicke model, $\lambda(t)$, to lead the system from a chaotic onto an integrable region, or viceversa. We do this change in two different ways: adiabatically and with finite rapidity. We proceed as follows.

Adiabatic evolution.- We assume that the conditions for the adiabatic theorem hold [41], and therefore the populations of the instantaneous eigenstates remain constant during this part of the protocol. This is possible because there are no real level crossings when changing λ —the integral of motion giving rise to the quantum number m', given in Eq. (12), is only approximate, and thus it is not possible to find degenerate energy levels [42, 43]. Hence, if the state is

$$|\psi\rangle = \sum_j c_j \, |E_j(\lambda[t_0])\rangle \, , \tag{13}$$

at the initial time t_0, then its time-evolved state, $|\psi(t)\rangle$, at any further time t is given by

$$|\psi(t)\rangle = \sum_j c_j \mathrm{e}^{-i\phi_j(t)} \, |E_j(\lambda[t])\rangle \, , \tag{14}$$

where $\phi_j(t)$ is the phase that each coefficent c_j acquires as a consequence of the adiabatic time evolution, and $|E_j(\lambda[t])\rangle$ denotes that each eigenstate is continuously changing. This phase only depends on the geometry of the energy levels‡,

$$\phi_j(\tau) = \int_0^\tau dt \, E_j(t). \tag{15}$$

If we assume a linear protocol between an initial value of the coupling constant, λ_i, and a final value, λ_f, that is $\lambda(t) = \lambda_i + (\lambda_f - \lambda_i)\, t/\tau$, then the acquired phases are

$$\phi_j = \frac{\tau}{\lambda_f - \lambda_i} \int_{\lambda_i}^{\lambda_f} d\lambda \, E_j(\lambda), \tag{16}$$

where $E_j(\lambda)$ is the value of the j-th eigenvalue of the Hamiltonian $H(\lambda)$.

As there is no way to analytically solve the integral in Eq. (16) —we would need the exact expression, $E_j(\lambda)$, for each energy level—, we get an approximation of the phases ϕ_j instead, by discretizing the integral given in Eq. (16) in finite steps with

‡ As our protocol consists in changing just one parameter, the net contribution of the geometrical Berry phase [44] is always zero, and therefore the only relevant contribution is given by the dynamical phase. See, for example, [45] for a detailed discussion of a similar protocol.

$\Delta\lambda = 10^{-2}$. We use $\tau = 10^5$ s, considering the experimental realization of the Dicke model discussed in [46], in which the frequencies ω and ω_0 are given in MHz.

Evolution with finite rapidity.- Solving the time dependent Schrödinger equation resulting from a time-dependent coupling constant, $\lambda(t)$, is highly demanding, specially for large characteristic times. An effective way to simulate this process consists in changing the coupling parameter by sudden, very small quenches, $\lambda_n \to \lambda_{n+1}$, with $\lambda_{n+1} = \lambda_n + \Delta\lambda$, ($|\Delta\lambda| \ll 1$), and letting the system relax after each quench. This implies that the time elapsed by the protocol is equal to the product of the number of quenches, N_λ, and the relaxation time after each quench, τ_λ, $\tau = N_\lambda \tau_\lambda$. All the numerical experiments shown in this paper are performed with $\tau_\lambda = 10^3$ μs. We have checked that similar results are obtained with larger values of τ_λ.

2.3. Notation

To facilitate the interpretation of the results presented in this paper, we summarize here the notation we use in the following sections.

Symbol	Meaning
$\left\langle \hat{O} \right\rangle$	Expected value of $\hat{O}$ in a particular state.
$\left\langle \hat{O} \right\rangle (t)$	Expected value of $\hat{O}$ in a time-evolving state.
$\left\langle \hat{O} \right\rangle_\infty$	Long-time average of the expected value of $\hat{O}$ in a time-evolving state.

Table 1. Summary of the notation using in this paper

The theoretical expression for $\left\langle \hat{O} \right\rangle_\infty$ is

$$\left\langle \hat{O} \right\rangle_\infty = \lim_{\tau\to\infty} \frac{1}{\tau} \int_0^\tau dt \, \langle\psi(t)| \hat{O} |\psi(t)\rangle \, . \tag{17}$$

However, as it is not possible to derive analytical expressions for this magnitude in the Dicke model, we rely on numerical estimates throughout all this paper,

$$\left\langle \hat{O} \right\rangle_\infty \simeq \frac{1}{N} \sum_{j=1}^{N} \left\langle \hat{O} \right\rangle (\tau + j\delta t), \tag{18}$$

for a large amount of time steps, N, and large values for τ and δt compared with the characteristic time scales of the systems. We take the experimental realization of the Dicke model proposed in [46] as a reference, so we consider that the characteristic time scales are given in μs. Therefore, values for τ and δt of the order of seconds are enough to obtain a good estimation of $\left\langle \hat{O} \right\rangle_\infty$ for any physical observable $\hat{O}$.

3. Thermalization and information

3.1. Preparation process

Our first step is to prepare two different equilibrium states to begin our numerical experiments. Both of them are based on the same idea: we start with the ground state of the Dicke model for a particular value of the coupling constant, λ_i; then, we quench it to a different value, $\lambda_i \to \lambda_f$, and finally we let the system relax at the final value of the coupling constant, λ_f, during a very large amount of time, $\tau = 10^5$s. Following this scheme, we prepare two different initial states:

State $|\psi_1\rangle$.- We start from the ground state of the Dicke model at $\lambda = 1.879$ and quench it to $\lambda = 1$.

State $|\psi_2\rangle$.- We start from the ground state of the Dicke model at $\lambda = 3.56$ and quench it to $\lambda = 2.2$.

As we will discuss later in detail, these two states are characterized by a totally different distribution of coefficents $|c_j|^2$. This is because the first preparation process leads the system onto a highly chaotic region, whereas the second one leads the system onto an approximately integrable region. This is the key element to observe important differences in theremalization, as we will discuss in the next sections.

3.2. Time evolution and equilibrium states

To perform a first test of thermalization, we adiabatically lead both $|\psi_1\rangle$ and $|\psi_2\rangle$ to the same value of the coupling constant, $\lambda = 0.8$. Both preparation processes are designed to reach the same value of the final energy, $E/j = -0.19$, which lays within the chaotic region of the Dicke model, both in its classical [36] and the quantum [47] versions. Results are shown in Fig. 1, for a system composed by $N = 40$ atoms. In this figure we show the time evolution of four different observables, $a^\dagger a$, $\left(a + a^\dagger\right)^2$, J_x^2 and J_z', at the final stage, $\lambda = 0.8$. The red curve displays the result obtained with the first state, $|\psi_1(t)\rangle$, and the green curve, the result obtained with the second state, $|\psi_2(t)\rangle$. The black dotted line represents the microcanonical average, Eq. (5), calculated with $\mathcal{N} = 41$ levels centered at the mean energy, $E/j = -0.19$. We can see that both preparations give rise to indistinguishable results, fluctuating around the microcanonical average with the same width. Taking into account that we are working with a pretty small system, with $N = 40$, these results suggest that both states are thermalized, and therefore that the differences between their preparation processes have been ruled out.

At this point, it is worth to remark that had we performed the same protocol with the classical version of the Dicke model, we would have obtained the same qualitative results. As we have pointed out above, the classical version of the Dicke model is highly chaotic at $\lambda = 0.8$ and $E/j = -0.19$. Hence, any trajectory is expected to explore the whole surface of constant energy, independently of its initial condition, under these circumstances. This means that long-time averages of physical observables are expected to give the same results for any initial condition. Hence, results displayed in Fig. 1 are

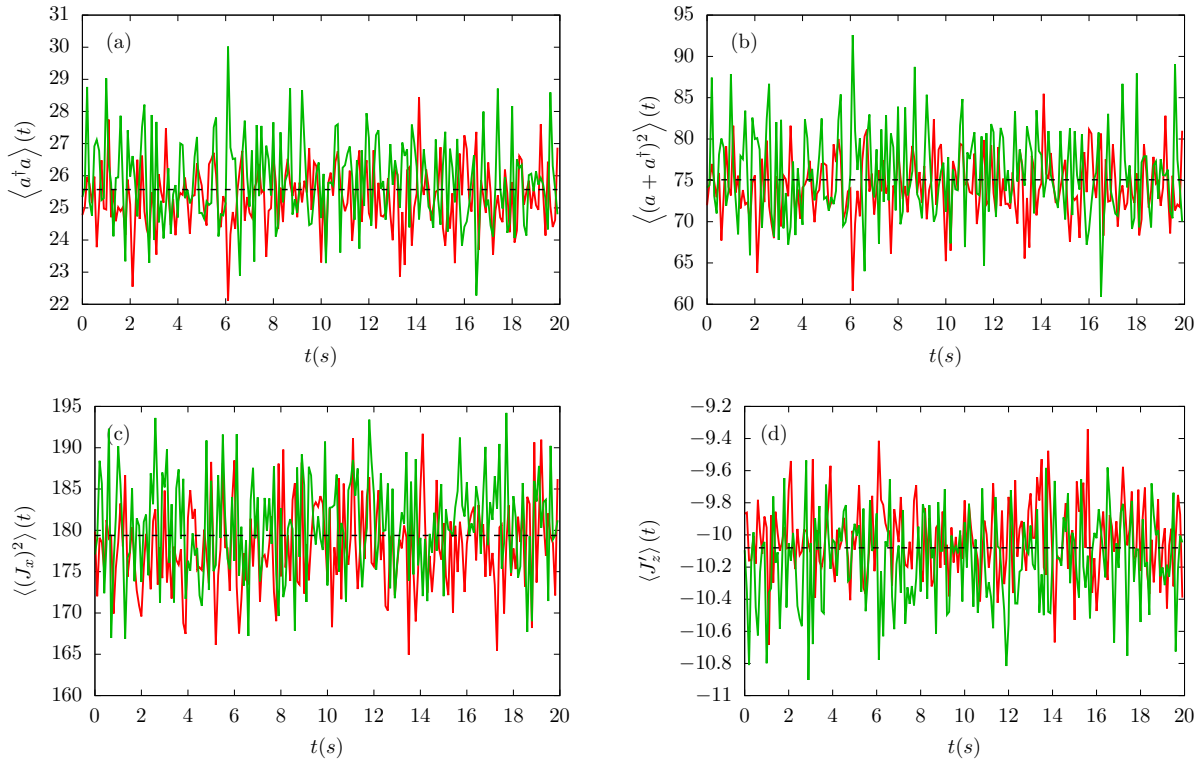

Figure 1. Time evolution of the expected values of $a^\dagger a$ [panel (a)], $\left(a^\dagger + a\right)^2$ [panel (b)], J_x^2 [panel (c)], and J_z' [panel (d)], at $\lambda = 0.8$. Red solid lines represent the result obtained with $|\psi_1(t)\rangle$; greed solid lines, the result obtained with $|\psi_2(t)\rangle$, and the black dotted line the microcanonical average, Eq. (5).

compatible with the same qualitative behavior happening in the classical realm.

Our second test consists in adiabatically leading both preparations from the situation displayed in Fig. 1, after evolving during $\tau = 10^5$ s at $\lambda = 0.8$, to the integrable region, $\lambda_i = 0.8 \to \lambda_f = 2.5$. In Fig. 2 we show what we observe in an intermediate stage of the adiabatic evolution§, at $\lambda = 2.2$. Here, we observe a number of remarkable facts:

(i) The results obtained with $|\psi_1(t)\rangle$ (red lines) and $|\psi_2(t)\rangle$ (green lines) are totally different, not only regarding their averages, but also their fluctuations.

(ii) Only $|\psi_1(t)\rangle$ is close to the microcanonical average (black dotted line).

(iii) Fluctuations in both J_x^2 and J_z' are very small. The fact that $J_z'(t)$ is almost constant in time indicates that we are in an approximately integrable region. This is consistent with the results published in [33, 34]. The energy for both $|\psi_1\rangle$ and $|\psi_2\rangle$ is $E/j = -6$ at $\lambda = 2.2$, and this point in the parameter space of the Dicke model lies within the approximate integrable region.

Again, a comparison with the same experiment performed with the classical version

§ As our protocol consists in approximating the integral in Eq. (16) in discrete steps with $\Delta\lambda = 10^{-2}$ and $\tau = 10^5$, the results shown in Fig. 2 can be understood as the first 20 s of the relative phases acquired at $\lambda = 2.2$.

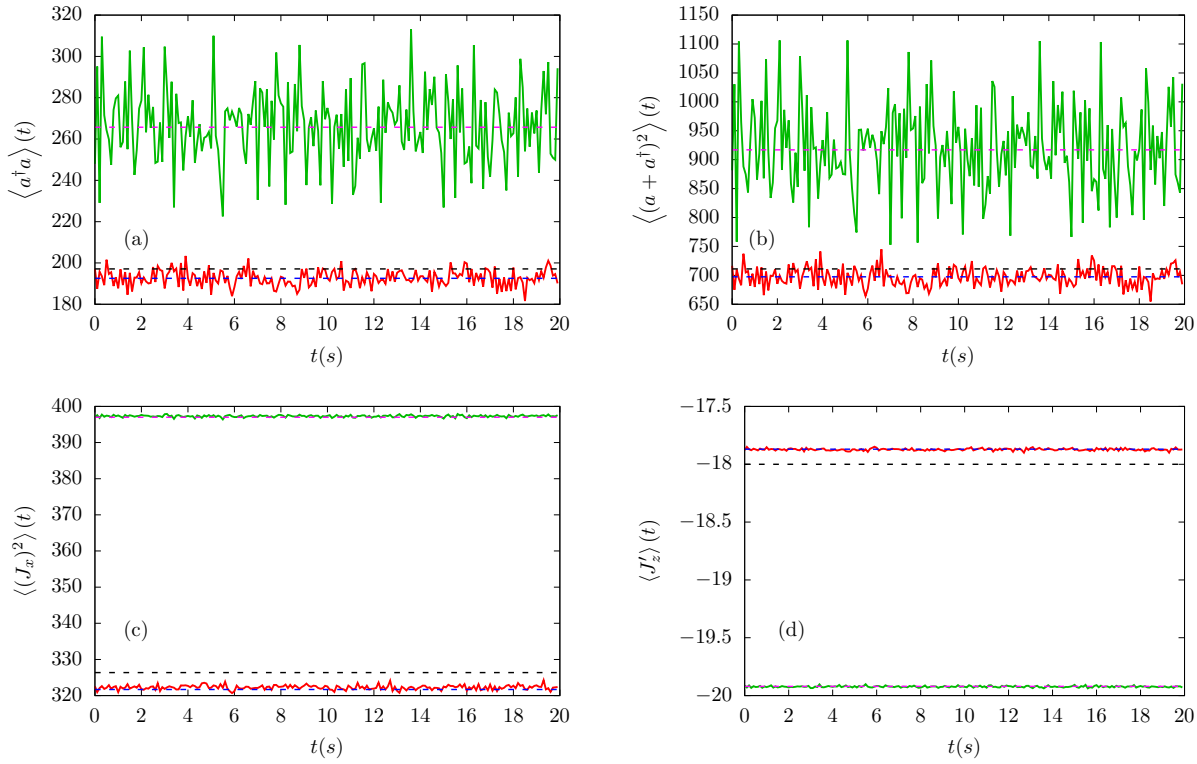

Figure 2. Time evolution of the expected values of $a^\dagger a$ [panel (a)], $\left(a^\dagger + a\right)^2$ [panel (b)], J_x^2 [panel (c)], and J_z' [panel (d)], at $\lambda = 2.2$. Red solid lines represent the result obtained with $|\psi_1(t)\rangle$; greed solid lines, the result obtained with $|\psi_2(t)\rangle$. The black dotted line display the microcanonical average, Eq. (5); the blue dotted line, the result of applying the generalized microcanonical ensemble, (21), to the state $|\psi_1(t)\rangle$, and the magenta dotted line, the result of applying the same ensemble to $|\psi_2(t)\rangle$.

of the Dicke model may shed some light on these results. Now, we are in an approximate integrable region. This means that every trajectory is attached to an integrable torus, and therefore long-time averages are expected to depend on the corresponding initial conditions. A first consquence of this fact is that the microcanonical average, which covers all the integrable tori, cannot be classically recovered. A second, and more subtle, consequence is the following. Let us imagine that we repeat the same experiment a large number of times. Due to the extreme sensitivity of initial conditions within the chaotic region, any tiny experimental uncertainty will be exponentially amplified during the protocol. Therefore, we can expect each realization of the experiment to finish in a different integrable torus, independently of the details of its preparation process. Hence, we cannot expect to identify the preparation process from which we start by means of equilibrium measurements at this stage of the experiment. And thus, we expect classical results to be totally different from the quantum results shown in Fig. 2.

All these results have been obtained with a single system size, $N = 40$. Hence, we can wonder how the differences between Figs. 1 and 2 change with the system size. To delve into this question, we shown in Fig. 3 some results obtained with four different

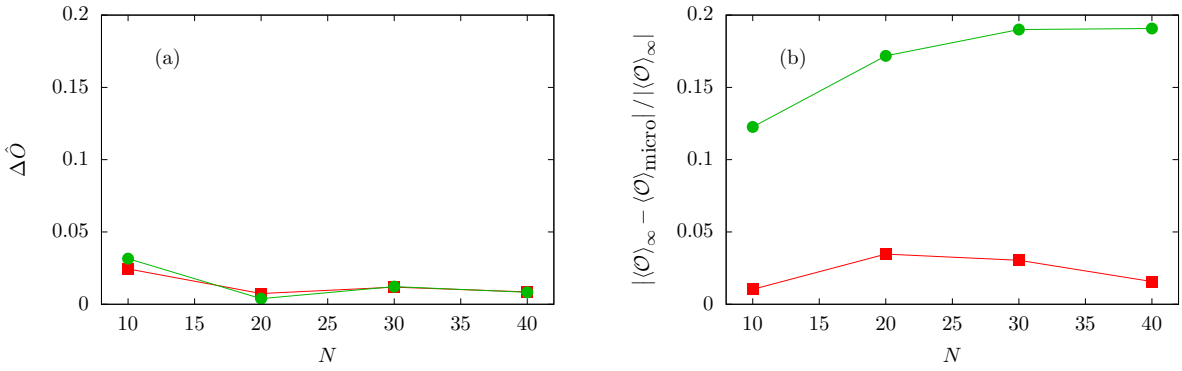

Figure 3. Mean relative differences between long-time and microcanonical averages, using the four observables shown in Figs. 1 and 2, as a function of the system size, N. Red symbols show the results with $|\psi_1\rangle$; green symbols, the results with $|\psi_2\rangle$. Panel (a) is obtained at $\lambda = 0.8$; panel (b), at $\lambda = 2.2$.

number of atoms, $N = 10$, $N = 20$, $N = 30$, and $N = 40$. In both panels we show how an average difference between long-time and microcanonical averages for a set of physical observables,

$$\Delta\hat{O} = \sum_{i=1}^{4} \frac{\left|\left\langle\hat{O}_i\right\rangle - \left\langle\hat{O}\right\rangle_{ME}\right|}{\left|\left\langle\hat{O}_i\right\rangle\right|}, \tag{19}$$

change with system size. We work with the same observables plotted in Figs. 1 and 2, $\hat{O}_1 = a^\dagger a$, $\hat{O}_2 = (a^\dagger + a)^2$, $\hat{O}_3 = J_x^2$, and $\hat{O}_4 = J_z'$. In panel (a) we show the results obtained at $\lambda = 0.8$, that is, at the same value used to obtain Fig. 1. We can see that the relative differences between long-time and microcanonical averages remain very small for both $|\psi_1\rangle$ and $|\psi_2\rangle$, showing no clear trends when increasing the system sizes. But the results shown in panel (b), corresponding to $\lambda = 2.2$, are completely different. Those obtained from $|\psi_1\rangle$ are very similar to the ones shown in panel (a). But this is not what happens with $|\psi_2\rangle$. In this case, the relative differences between long-time and microcanonical averages are very large and show no signatures of decreasing when increasing the system size. Hence, and even though it is not possible to deal with much larger systems with current computational capabilities, these results suggest that the non-thermalizing behavior of $|\psi_2\rangle$ may survive in the thermodynamic limit.

3.3. How much information is encoded in the equilibrium states?

The explanation of the differences between the results shown in Fig. 2 and what is expected for a classical system lays in the coefficents $|c_j|^2$, which remain constant during all the adiabatic process. To delve into this fact, we take into account that J_z' is now a very approximate constant of motion. Therefore, standard thermalization is not expected because both the energy and J_z' are conserved by the unitary evolution. Under such circumstances, equilibrium states are usually well described by the Generalized Gibbs Ensemble (GGE) [48], which depends on two intesive thermodynamic magnitudes:

the standard (inverse) temperature, β, and a generalized temperature, γ, associated to J'_z,

$$\rho_{GGE} = \frac{1}{Z} \mathrm{e}^{-\beta H - \gamma J'_z}. \tag{20}$$

This ensemble can be understood as a generalization of the canonical (or Gibbs) ensemble, formulated for systems in contact with a thermal bath. If $[H, J'_z] = 0$, J'_z is diagonal in the eigenbasis of the Hamiltonian.

Although GGE provides a very accurate description of equilibrium states in integrable systems, we find two important caveats regarding its application to our numerical experiments. First, our system remains thermally isolated, and its size is not large enough to guarantee the equivalence between Gibbs and microcanonical ensembles. Second, J'_z is only an approximate constant of motion. Therefore, J'_z is not exactly diagonal in the eigenbasis of the Hamiltonian, and hence Eq. (20) may include (small) non-diagonal terms. As a consequence, and even though a generalization of the GGE to isolated systems has been derived [49], we propose a different ensemble to account for the role played by J'_z. We follow the ideas proposed in [50, 51], to build an ensembe based on: *(a)* as in the standard microcanonical ensemble, only a small window, ΔE, around the conserved energy, E, is populated; *(b)* the population of the energy levels inside this window is obtained by maximizing the entropy of the resulting ensemble, ρ_{GM}, conditioned to $\langle J'_z \rangle_\infty = \mathrm{Tr}\left[\rho_{GM} J'_z\right]$. These ideas lead to

$$\rho_{GM}(E, \gamma) = \frac{1}{Z} \sum_{n|E_n \in [E, E+\Delta E]} \mathrm{e}^{-\gamma J'_{z,n}} \left|E_n\right\rangle \left\langle E_n\right|, \tag{21}$$

where $J'_{z,n} = \left\langle E_n\right| J'_z \left|E_n\right\rangle$, and $Z = \sum_{n|E_n \in [E, E+\Delta E]} \mathrm{e}^{-\gamma J'_{z,n}}$. Note that this ensemble does not really depend on J'_z, but on a slightly different magnitude:

$$\widetilde{J}_z = \sum_{mn} \left\langle E_m\right| J'_z \left|E_n\right\rangle \delta_{mn} \left|E_m\right\rangle \left\langle E_n\right|. \tag{22}$$

By definition, this operator is always diagonal in the eigenbasis of the Hamiltonian, and therefore it always fulfills $[H, \widetilde{J}_z] = 0$, so then $\left\langle \widetilde{J}_z \right\rangle_\infty = \left\langle \widetilde{J}_z \right\rangle (t)$, $\forall t$. Hence, when J'_z is a very approximate constant of motion, $J'_z \sim \widetilde{J}_z$, and therefore the parameter γ in Eq. (21) accounts for the role that J'_z plays in the equilibrium state. On the contrary, within a chaotic region, γ accounts for the role played by the *artificial* constant of motion, $\widetilde{J}_z$. It has been shown that although these kind of artificial constants of motion can be always built in chaotic quantum systems, they do not provide a valuable description of equilibrium states [52]. Anyhow, it is worth remarking that the standard microcanonical ensemble is recovered when $\gamma = 0$; in such a case, the equilibrium state keeps no information about the expected value of the second constant of motion, either J'_z or $\widetilde{J}_z$. On the contrary, $\gamma \neq 0$ indicates that the equilibrium state depends on it.

In all the panels of Fig. 2 we display the results of applying Eq. (21). Blue dotted lines are calculated with the value of γ obtained from $|\psi_1\rangle$, $\gamma_1 = -6.46 \cdot 10^{-2}$; magenta dotted lines display the result for $|\psi_2\rangle$, $\gamma_2 = 3.78$. In both cases, the microcanonical

energy window is composed by $\mathcal{N} = 41$ energy levels centered at $E/j = -6$, and γ is calculated by solving

$$\mathrm{Tr}\left[\rho_{GM}(E,\gamma)J'_z\right] = \langle J'_z\rangle_\infty \,. \tag{23}$$

Note that $\rho_{GM}(E,\gamma)$ exactly reproduces $\langle J'_z\rangle_\infty$ by definition. Hence, to determine whether this ensemble provides a better description of equilibrium states that the standard microcanonical ensemble or not, we must study other observables, as it is done in panels (a), (b) and (c) of Fig. 2.

We obtain two remarkable results:

(i) Eq. (21) provides very accurate results for both $|\psi_1\rangle$ and $|\psi_2\rangle$, and the four physical observables.

(ii) γ_1 is close to zero. This means that the first preparation procedure keeps almost no information about J'_z. On the contrary, γ_2 is very large. This means that the second preparation procedure only populates the energy levels with very small values of $\langle J'_z\rangle$. Specifically, $\gamma_2 = 3.78$ implies that the population of energy levels with $\langle J'_z\rangle = -j = -20$ is 43.8 times larger than the poulation of energy levels with $\langle J'_z\rangle = -j+1 = -19$. Taking into account that the initial states of both preparation procedures —the ground state of the Dicke model at $\lambda = 1.879$ for $|\psi_1\rangle$, and the ground state at $\lambda = 3.56$ for $|\psi_2\rangle$— have $\langle J'_z\rangle = -j = -20$, this means that *the information about the initial value of* $\langle J'_z\rangle$ *is still present in* $|\psi_2\rangle$*, even though it seemed thermalized at* $\lambda = 0.8$*, and it stayed for a very long time within a strongly chaotic region.*

To get a more complete picture, we study how long-time averages of physical observables change with λ as the adiabatic protocol from $\lambda_i = 0.8$ to $\lambda = 2.5$ is done. In Fig. 4 we show the results for $a^\dagger a$ and J'_z; the results for the other two observables, $\left(a + a^\dagger\right)^2$ and J_x^2 follow the same pattern. Time averages are obtained using 200 different values of time from $t = 0$ to $t = 20$ s, after a relaxation time equal to $\tau = 10^5$ s —the same values we have displayed in Figs. 1 and 2. We also show the microcanonical average, Eq. (5), and the generalized microcanonical average, Eq. (21).

Panels (a) and (c) of Fig. 4 show that the standard microcanonical ensemble provides an accurate description for the results obtained with $|\psi_1\rangle$. The description obtained with the generalized microcanonical ensemble, Eq. (21), is slightly better, but given the small size of the system, $N = 40$, this fact can be a consequence of finite-size effects. On the contrary, panels (b) and (d) show that the description provided by the microcanonical ensemble is far from good for $|\psi_2\rangle$. If $\lambda \in (0.8, 1.8)$, both the time average, and the microcanonical and generalized microcanonical ensembles give the same results. But important differences emerge at larger values of the coupling constant. Both time average and the generalized microcanonical ensemble show oscillations that become very important when $\lambda > 1.9$. And, as expected from panels (a) and (c), the microcanonical ensemble does not account for them.

These oscillations also appear in parameter γ of Eq. (21). This is shown in panel (a) Fig. 5. We can distinguish three different regions in this plot. For $1.4 < \lambda < 1.9$, both γ_1 and γ_2 are roughly equal to zero, and show almost no fluctuations. For lower

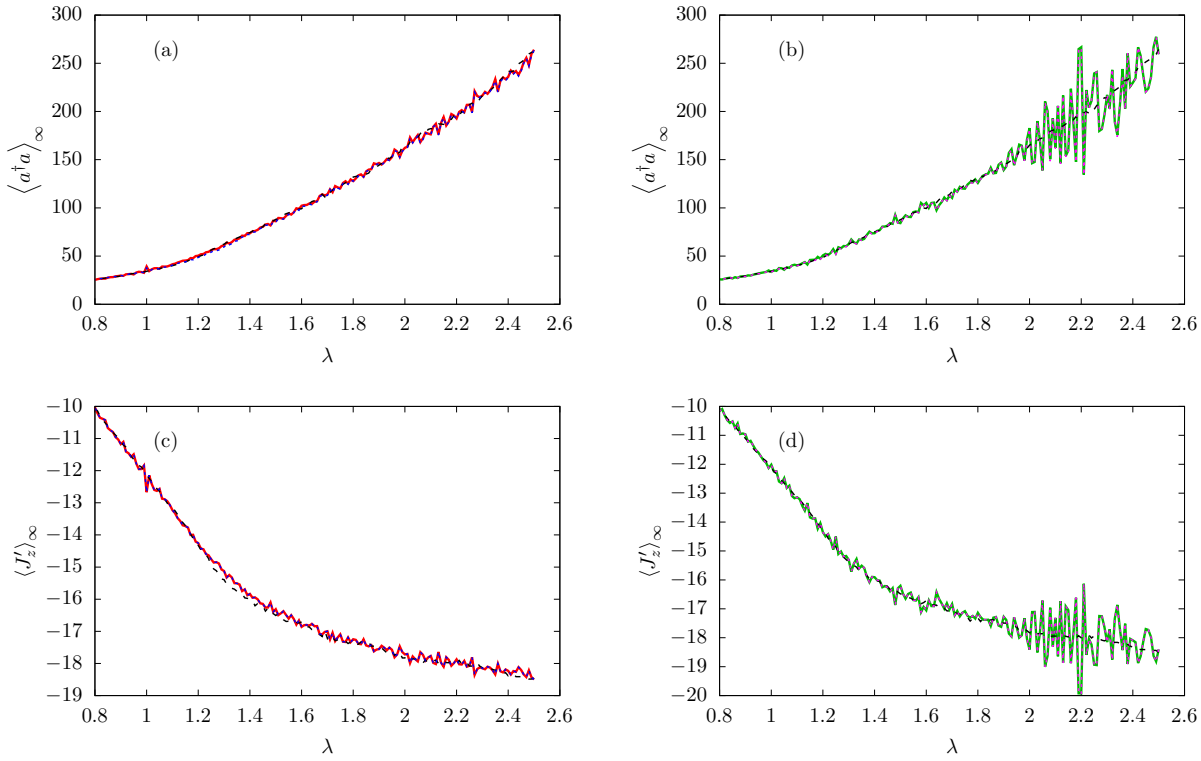

Figure 4. Comparison between time averages of relevant observables, and the predictions of both the standard microcanonical ensemble, Eq. (5), displayed with black dotted lines, and the generalized microcanonical ensemble, Eq. (21), displayed with blue dotted lines when it is obtained from $|\psi_1\rangle$, and with magenta dotted lines when it is obtained from $|\psi_2\rangle$. Time averages are plotted with red lines for $|\psi_1\rangle$, and with green lines for $|\psi_2\rangle$. Panel (a) shows the results for $a^\dagger a$ and $|\psi_1\rangle$; panel (b), the results for $a^\dagger a$ and $|\psi_2\rangle$; panel (c), the results for J'_z and $|\psi_1\rangle$, and panel (d), the results for J'_z and $|\psi_2\rangle$.

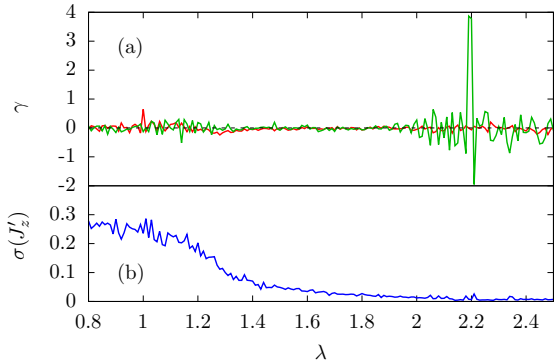

Figure 5. Panel (a), values for parameter γ in Eq. (21), for $|\psi_1\rangle$ (red line) and $|\psi_2\rangle$ (green line). Panel (b), size of the time fluctuations in $\langle J'_z \rangle(t)$, given by Eq. (24).

values of λ, mainly for $0.9 < \lambda < 1.3$ we can see larger fluctuations in both γ_1 and γ_2, despite the high degree of chaos. This is probably linked to the excited-state quantum phase transition, happening in the Dicke model at $E/j = -1$ for $\lambda > 0.5$, a value reached around $\lambda \sim 1.2$ with our protocol, and which induce non-analytical changes in both the density of states and the expected values of observables [29, 30, 31, 32]. Finally, for larger values of λ, $1.9 < \lambda < 2.5$, we can see that γ_1 is always close to zero, whereas γ_2 suffers from strong fluctuations, ranging from $\gamma_2 \sim -2$, to $\gamma \sim 4$.

In panel (b) of the same figure we show the size of the fluctuations in time of $\langle J'_z \rangle (t)$, in order to estimate the degree of integrability of the time evolution. In particular, we show

$$\sigma(J'_z) = \sqrt{\frac{1}{200} \sum_{k=1}^{200} \left(\langle J'_z \rangle (0.1k) - \langle J'_z \rangle_\infty \right)^2}, \tag{24}$$

that is, an estimate of the variance of the fluctuations in time of $\langle J'_z \rangle (t)$. It is worth to remark here that this average is performed over a period of 20 s, which is very long considering that the frequencies ω and ω_0 are given in MHz, as discussed above. As $\sigma(J'_z) = 0$ in the integrable limit, in which $[H, J'_z] = 0$, we can see how the time evolution is slowly becoming more chaotic as the coupling constant is decreased in the region $1.4 < \lambda < 2.5$. Then, the time fluctuations of $\langle J'_z \rangle (t)$ fast increase up to $\lambda = 1$, below which they remain approximately constant. This suggest that full chaos is developed at this value of the coupling constant, and that the great majority of the transition from approximate intregrability to chaos takes place between $\lambda = 1.4$ and $\lambda = 1$.

We can link the fluctuations in the parameter γ in the region $1.9 < \lambda < 2.5$, which lies within the approximate integrable region, to the changes in the values of $\langle E_n | J'_z | E_n \rangle$ as the coupling constant λ is modified by the protocol. This is illustrated in Fig. 6. We plot there the evolution of five energy levels with positive parity‖ for a small region close to $\lambda = 2.2$. We highlight in red the most populated energy level, that is, the eigenstate for which $|c_j|^2 = |\langle E_n | \psi(0) \rangle|^2$ is maximum; this eigenstate is $\left| E^+_{195} \right\rangle$, where the superindex + indicates that it is the 195th energy level with positive parity. In panel (a) of this figure we show the evolution of the energy values for each one of these eigenstates; in panel (b), the corresponding values of $\langle E_n | J'_z | E_n \rangle$. Let us focus our attention in what happens around $\lambda \approx 2.2027$. At this point, $\left| E^+_{195} \right\rangle$ and $\left| E^+_{194} \right\rangle$ have almost the same energy —they experiment an avoided level crossing. We can see in panel (b) of Fig. 6 that they swap the values of $\langle E_n | J'_z | E_n \rangle$ at this value of the coupling constant: $\left\langle E^+_{195} \right| J'_z \left| E^+_{195} \right\rangle$ changes from -20 to -16, and the opposite happens for $\left| E^+_{194} \right\rangle$. As a consequence of this fact, we would observe a change from $\langle J'_z \rangle (t) = -20$ to $\langle J'_z \rangle (t) = -16$ when crossing $\lambda = 2.2027$ in a numerical experiment with an initial condition equal to $\left| E^+_{195} \right\rangle$. We can see in panel (b) of Fig. 4 that this very same phenomenon happens in our numerical experiment, even though the initial condition is not equal to $\left| E^+_{195} \right\rangle$, but it spreads over a large number of eigenstates. This

‖ As $[H(\lambda), \Pi] = 0$, $\forall \lambda$, the transitions between eigenstates with different parity are forbiden, and therefore real crossings between eigenstates belonging to different parity sectors imply no consequences.

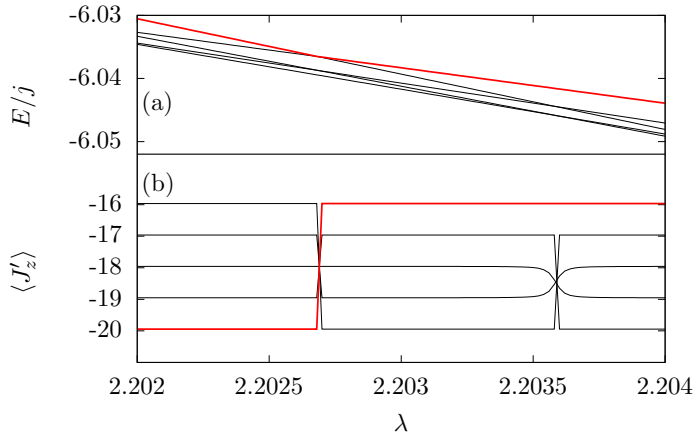

Figure 6. Avoided level crossings around $\lambda = 2.2$. Panel (a) shows the values of five energy levels as a function of λ; the red line indicates the most populated energy level. Panel (b) shows the expected value of $\langle J'_z \rangle$ in the corresponding eigenstates.

happens because all the energy levels with $\langle E_n | J'_z | E_n \rangle = -20$ experiment the same kind of avoided level crossing at $\lambda = 2.2027$, and all of them change to $\langle E_n | J'_z | E_n \rangle = -16$ at this particular value of the coupling constant. It is worth to note that this is an exceptional phenomenon; the great majority of avoided level crossings involve one or just a few energy levels. As a consequence, passing through different avoided level crossings normally entails jumps to different values of the quantum number m'. And therefore, the time-evolved wavefunction, $|\psi_2(t)\rangle$, becomes a supperposition of different values of j' after passing through a number of them, so its behavior becomes similar to the microcanonical ensemble. However, it is worth noting that this fact does not entail the erasure of the information about J'_z encoded in the initial state. This information is still there, but it is hidden due to the *re-shuffling* of the values of $\langle J'_z \rangle$. We will come back to this point in the next section.

To delve into this conclusion, we display in Fig. 7 the *Peres lattices* for J'_z and different values of λ. These lattices were introduced by A. Peres in 1984 to describe the onset of chaos [53]. They consist in diagrams representing the expected value of observables in the eigenstates of the Hamiltonian, in this case $\langle E_n | J'_z | E_n \rangle$. In the integrable limit, this diagram gives rise to a regular pattern, because J'_z approximately commutes with the eigenstates, $[J'_z, |E_n\rangle \langle E_n|] \sim 0$, and every eigenstate is characterized by the corresponding quantum number, m'. On the contrary, in the chaotic region $[J'_z, |E_n\rangle \langle E_n|] \neq 0$, and the same diagram shows an erratic pattern. In Fig. 7 we show results for $\lambda = 2.2$, 1.8, 1.4, and 1. The energy levels between the red (green) lines are those which represent the 90% of the wavefunction of $|\psi_1\rangle$ ($|\psi_2\rangle$). The diagram corresponing to $\lambda = 2.2$ shows that the Dicke model is approximately integrable within the energy region at which the adiabatic evolution takes place. The plot for $\lambda = 1.8$ shows that integrability is starting to break down at this value of the coupling constant; although the pattern is still ordered, we can see deviations from the expected values

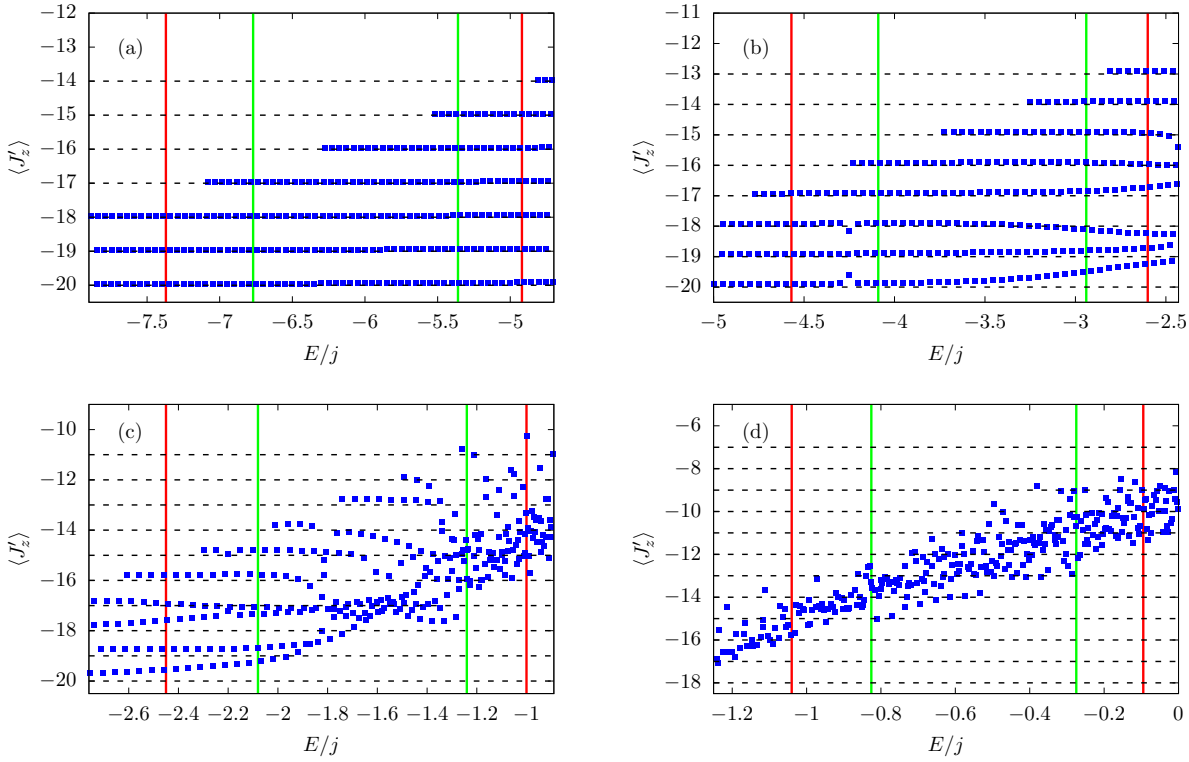

Figure 7. Peres lattices for $\langle J'_z \rangle$ and different values of λ: panel (a) shows $\lambda = 2.2$; panel (b), $\lambda = 1.8$; panel (c), $\lambda = 1.4$, and panel (d), $\lambda = 1$. Black dotted lines indicate the expected values for a perfect integrable system, $\langle J'_z \rangle = -j, -j+1, \ldots, j$. The population of the energy levels between the two vertical red lines sum the 90% of the state $|\psi_1\rangle$. The vertical green lines indicate the 90% of the state $|\psi_2\rangle$.

of J'_z if $[J'_z, |E_n\rangle \langle E_n|] = 0$ (shown as black dotted lines). The scenario is completely different for $\lambda = 1.4$ and $\lambda = 1$. For this last case, $\langle E_n| J'_z |E_n\rangle$ conform a cloud of points, with no traces of regularity.

This figure reinforces our previous statement claiming that avoided level crossings force $|\psi_2\rangle$ to behave like the standard microcanonical ensemble before reaching a highy chaotic regime, which we can settle now between $\lambda = 1.4$ and $\lambda = 1$. Furthermore, panels (a) and (d) also provide an explanation for the different behavior of $|\psi_1\rangle$ and $|\psi_2\rangle$ around $\lambda = 2.2$. The first one is obtained by quenching system to the scenario displayed in panel (d). As J'_z is no longer a constant of motion for that value of the coupling constant, there are no forbiden transitions between the initial and final Hamiltonians, and therefore the coefficents $|c_j|^2$ become approximately random, and do not keep information about the initial value of J'_z. On the other hand, $|\psi_2\rangle$ is obtained by a quench to $\lambda = 2.2$, displayed in panel (a). In this case, J'_z is still a very approximate constant of motion. Therefore, the transitions from the ground state of the Dicke model at $\lambda = 3.56$ to eigenstates of the same model at $\lambda = 2.2$ with $\langle E_n| J'_z |E_n\rangle \neq -20$ are forbidden, and therefore the resulting distribution of coefficents $|c_j|^2$ is regular and stores a lot of information about the initial value of J'_z. As the rest of the evolution is adiabatic, this information is not

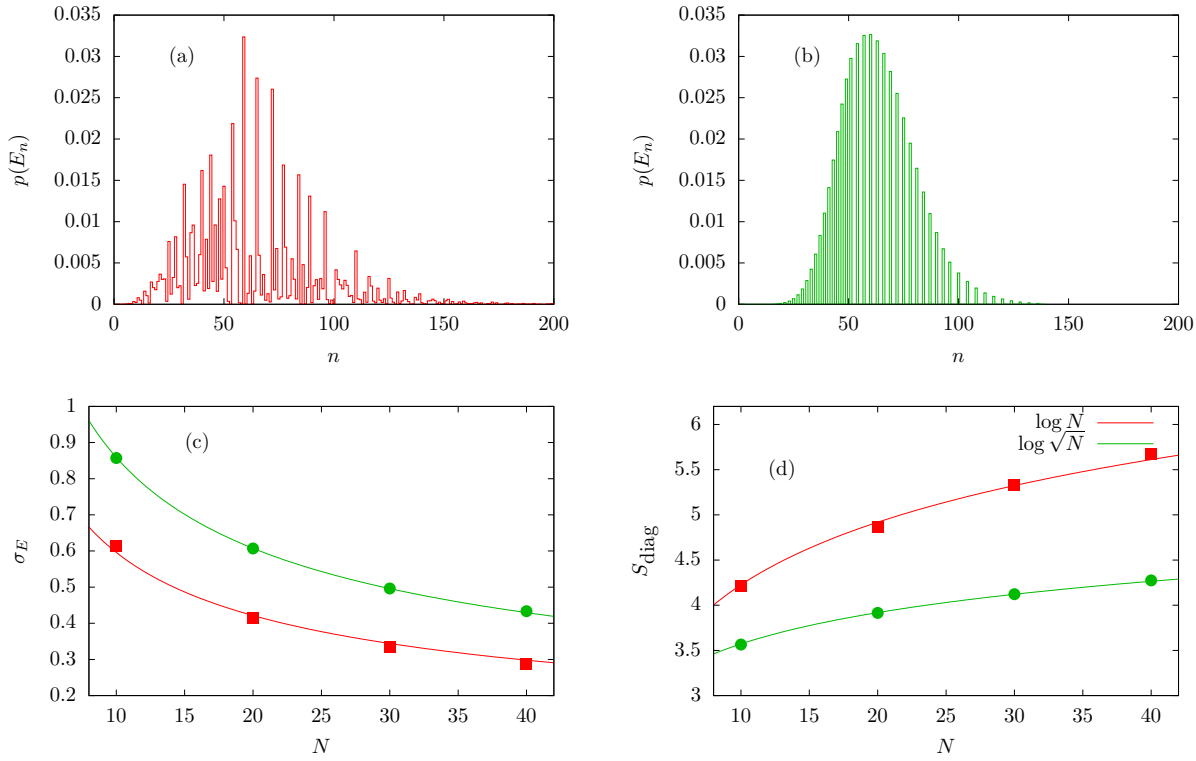

Figure 8. Panel (a) distribution of coefficents $|c_j|^2 = P(E_n)$, where $P(E_n)$ is the probability of obtaining E_n when measuring the energy, for the state $|\psi_1\rangle$ and $N = 20$. Panel (b), the same distribution for the state $|\psi_2\rangle$ and $N = 20$. Panel (c), energy width of both $|\psi_1\rangle$ (red squares) and $|\psi_2\rangle$ (green circles) as a function of the system sizes. The solid lines display the main trend, $\sigma_E \propto N^{-1/2}$. Panel (d), diagonal entropy for both $|\psi_1\rangle$ (red squares) and $|\psi_2\rangle$ (green circles), as a function of the system size. The red solid line represents the main trend for $|\psi_1\rangle$, $S_{\rm diag} \propto \log N$, and the green solid line, the main trend for $|\psi_2\rangle$, $S_{\rm diag} \propto \log \sqrt{N}$.

erased, even though it is not visible when the system is chaotic and the ETH scenario holds. A first conclusion is that $|\psi_1\rangle$ *is much better thermalized than* $|\psi_2\rangle$*, although this difference cannot be determined by equilibrium measurement within a chaotic region.*

A complementary test for this claim is given in Fig. 8. In panels (a) and (b) we show the distribution of coefficents $|c_j|^2$ for $|\psi_1\rangle$ and $|\psi_2\rangle$; in both cases, $N = 20$. We can see clear differences between these two histograms. The shape of the first one suggests that the eigenstates of the Dicke model at $\lambda = 1$ have been randomly populated in a small window around the mean energy E, as a consquence of the quench. On the contrary, the distribution for $|\psi_2\rangle$ show a clear pattern: the eigenstates with $\langle E_n| J'_z |E_n\rangle \neq -10$ are not populated at all (note that we display a case with $N = 20$ in these two panels), and the population of the levels with $\langle E_n| J'_z |E_n\rangle = -10$ is a smooth function of the energy. To study the consequences of these facts and how they change with the system size, we display the width, σ_E, of these distributions in panel (c), and their diagonal entropy, $S_{\rm diag} = -\sum_j |c_j|^2 \log |c_j|^2$, in panel (d). We can see that $\sigma_E \propto N^{-1/2}$ in

both cases, as expected for thermalizing systems. Thus, the faliure of thermalization observed for $|\psi_2\rangle$ at $\lambda = 2.2$ is not related to the energy width of the state, but to the selective population of different eigenstates as a consequence of the quench. This claim is reinforced by the results for the diagonal entropy, displayed in panel (d). We can see that this magnitude grows with $\log N$ for $|\psi_1\rangle$, and with $\log\sqrt{N}$ for $|\psi_2\rangle$. This means that the second preparation process always populates a smaller number of energy levels than the first one, due to the conservation of J_z' during the quench. Thus, even though it is not possible to simulate very large systems with the current computational capabilities, we can conjecture that the differences between $|\psi_1\rangle$ and $|\psi_2\rangle$ survive in the thermodynamic limit.

4. Information erasing mechanism

The main result of the previous section is that it is possible to prepare a thermalized state, within a chaotic region, which stores a relevant amount of information about its past, information that emerges by adiabatically leading the system to a particular integrable region. But it is easy to see that this claim suffers from two important shortcomings. First, it has been inferred from just one numerical experiment. Second, no real time evolution has been performed; we have just simulated an adiabatic evolution. As we have pointed out above, this is what we expect if the time-dependent process is slow enough... but, what does this exactly mean? Is it possible to perform such a slow experiment? In other words, is it possible to complete our proposal under realistic experimental conditions?

To deal with this question, we work with $|\psi_2\rangle$ to carry out a cyclic processes $\lambda = 2.2 \to \lambda = 1 \to \lambda = 2.2$ with finite rapidity, and to study the differences between the initial and the final states, both at $\lambda = 2.2$. As we have discussed in the previous section, the initial state of this protocol, $|\psi_2(0)\rangle$, verifies $\langle\psi_2| J_z' |\psi_2\rangle = -j$, and therefore its equilibrium properties are well described by the generalized microcanonical ensemble, Eq. (21), with a large value of γ. This means that it stores a large amount of information about the preparation process. As this protocol requires much more computational effort than the one performed in the previous section, we work with a smaller systems, with $N = 6$ and $N = 8$ atoms, and we focus on the energy and just one observable, $a^\dagger a$, which is diagonal in the Fock basis and therefore easy to calculate. That is, our aim is to study the differences between the initial and final values of the energy and $\left\langle a^\dagger a \right\rangle_\infty$ as a function of the duration of the process, τ. To perform a kind of ensemble average, we work with 10 different realizations of the same process, characterized by its duration, τ. Before the cycle starts, we let the system relax at $\lambda = 2.2$ during a time $\tau_i = 10^3 + r_i$ μs, where r_i is a Gaussian random number of mean $\mu = 0$ and variance $\sigma = 1$. That is, we build an ensemble of equivalent processes of durantion τ, relying on 10 initial states differing only in a tiny part of their relaxation times before the cycle starts.

Results are shown in Fig. 9. In panel (a), we show the energy at the end of the cycle, E/j, as a function of the time elapsed by the protocol, for both $N = 6$ (magenta

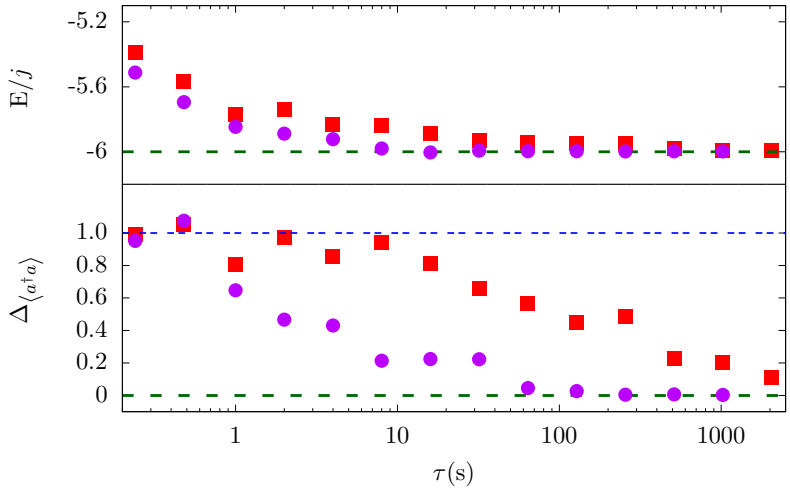

Figure 9. Final values of E/j (upper panel) and the scaled difference between $\langle a^\dagger a\rangle_\infty$ and the prediction of the microcanonical ensemble, $\Delta_{\langle a^\dagger a\rangle}$ (lower panel), after an average of 10 cycles $\lambda = 2.2 \to \lambda = 1 \to \lambda = 2.2$, started from $|\psi_2\rangle$, and versus the characteristic time of the process. Magenta circles show the results for $N = 6$, and red squares results for $N = 8$. In panel (a), the greed dashed line shows the initial value for the energy $E/j = -6$. In panel (b), the green dashed line shows the initial value for the expected value of the number of photons, corresponding to $\Delta_{\langle a^\dagger a\rangle} = 0$, and the blue dashed line shows the value obtained by a microcanonical average, corresponding to $\Delta_{\langle a^\dagger a\rangle} = 1$.

circles) and $N = 8$ (red squares). We find no surprises in this part of the figure. If the protocol is fast, the system is heated and the final energy is larger than the initial one, $E/j = -6$ (shown with a green dashed line in the figure); if it is slow, there is almost no dissipation and therefore the protocol approaches its adiabatic limit. We can also see that energy dissipation clearly grows with the number of atoms. For $N = 6$, it suffices a cycle time of $\tau = 10$ s to get rid of any dissipation; for $N = 8$, a much larger amount of time, $\tau = 100$ s, is required to obtain a similar result.

In panel (b) of the same figure, we show the results for the expected value of the number of photons, $\left\langle a^\dagger a\right\rangle_\infty$. As this number is extensive, we display a scaled difference betweem this expected value and the microcanonical average,

$$\Delta_{\langle a^\dagger a\rangle} = \frac{\left\langle a^\dagger a\right\rangle(0) - \left\langle a^\dagger a\right\rangle_\infty}{\langle a^\dagger a\rangle(0) - \langle a^\dagger a\rangle_{ME}}, \tag{25}$$

where $\left\langle a^\dagger a\right\rangle_{ME}$ represents the microcanonical average of the number of photons, and $\left\langle a^\dagger a\right\rangle(0)$ the initial value of this observable. That is, $\Delta_{\langle a^\dagger a\rangle} = 1$ if the equilibrium value of the number of photons equals the microcanonical average at the end of the cycle, and $\Delta_{\langle a^\dagger a\rangle} = 0$ if this equilibrium value equals its initial value at the end of the protocol. As a visual reference, we display $\Delta_{\langle a^\dagger a\rangle} = 1$ with a blue dashed line, and $\Delta_{\langle a^\dagger a\rangle} = 0$ with a green dashed line. The results shown here are more challenging that the ones displayed in panel (a). We can see that for very short times $\left\langle a^\dagger a\right\rangle_\infty$ approximately coincides with

the microcanonical average, as expecetd for a chaotic classical system. In this case, due to extreme sensitivity to initial conditions, a small difference in the initial state should be exponentially increased in the chaotic part of the protocol. Hence, its backward part should be totally different for each initial condition, and an average over a large number of them should coincide with the microcanonical average. It is worth to emphasize that this classical scenario does not depend on the time elapsed by the protocol —it occurs because the system passes through a highly chaotic region, independently of the protocol durantion τ. Results shown in panel (b) of Fig. 9 show that this is not what happens in our numerical experiment. As the protocol is slowed, both the cases with $N = 6$ and $N = 8$ atoms start to deviate from the microcanonical average, gradually recovering the initial values of the photon number. We can see that $\tau = 100$ s is enough to obtain $\left\langle a^\dagger a \right\rangle_\infty = \left\langle a^\dagger a \right\rangle (0)$ for $N = 6$. This means that the ten different trajectories end with the same number of photons that they had at the beginning of the protocol, even though the system stays during a very long time within a highly chaotic region. We can also see that the larger the number of atoms, the more difficult to reach this limit. For $N = 8$ we require a protocol durantion larger than $\tau = 1000$ s to recover the initial value of the number of photons.

From Fig. 9 we can gather two conclusions. First, the main results of the previous section are recovered if the durantion of the process, τ, is large enough. And second, there exists an information erasing mechanism that depends on the value of τ. Contrary to what happens in classical mechanics, where the information about the details of the initial state is ruled out as soon as the system enters in a chaotic region, this mechanism appears as a consequence of the changes in the system Hamiltonian during the protocol, and its efficency decays as its durantion is increased. To delve into this point, we perform a stringent fast numerical experiment, with $\tau = 3$s and $N = 8$. As it is shown in Fig. 9, energy dissipation is not very large for this protocol durantion, but the final value for $\left\langle a^\dagger a \right\rangle_\infty$ is very close to the microcanonical ensemble, meaning that the information about the details of the preparation process is ruled out at the final stage of the cycle; a fit to Eq. 21 gives rise to $\gamma \sim 0$. We complete the cycle, $\lambda = 2.2 \to \lambda = 1 \to \lambda = 2.2$, with 1000 different initial conditions, and study the sensitivity to their details. In particular, we analyze the variability of $\left\langle a^\dagger a \right\rangle_\infty$.

Main results are displayed in Fig. 10. Panel (a) shows a level diagram of a selection of the most populated energy levels as a function of λ. Vertical dashed lines indicate the values of λ at which avoided level crossings occur within the approximate integrable region. As we have pointed out above, in each of these points, two eigenstates swap their properties. It is important to remark that they are not exactly degenerate because the quantum number m' is not exact [42, 43]. Panel (b) shows the standard deviation of $\sigma_{\langle a^\dagger a \rangle}$,

$$\sigma_{\langle a^\dagger a \rangle} = \frac{1}{N} \sum_{j=1}^{N} \left(\left\langle a^\dagger a \right\rangle_{\infty,j} - \overline{\langle a^\dagger a \rangle} \right)^2 , \tag{26}$$

where the sum is over $N = 1000$ different realizations, $\left\langle a^\dagger a \right\rangle_{\infty,j}$ represents the expected

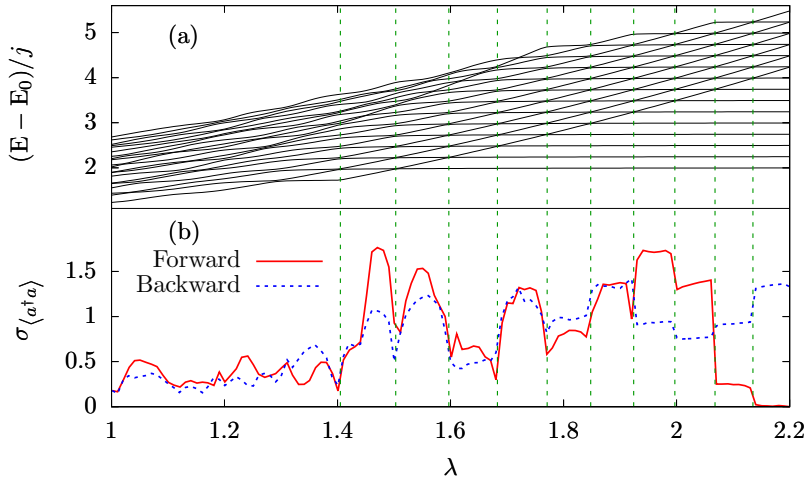

Figure 10. Panel (a), 21 selected energy levels for a system with $N = 8$ atoms. Panel (b), standard deviation of $\langle a^\dagger a\rangle_\infty$, among $N = 1000$ different realizations.

value of $a^\dagger a$ in the j-esim realization, and $\overline{\langle a^\dagger a\rangle}$ is the average over all the $N = 1000$ realizations,

$$\overline{\langle a^\dagger a\rangle} = \frac{1}{N}\sum_{j=1}^{N} \left\langle a^\dagger a\right\rangle_{\infty,j} . \tag{27}$$

We highlight the following facts. First, all the realizations give rise to almost the same value for $\left\langle a^\dagger a\right\rangle_\infty$ up to the value of λ at which the first avoided crossing occurs, $\lambda \simeq 2.13$. And second, $\sigma_{\langle a^\dagger a\rangle}$ abruptly changes every time an avoided crossing takes place. This is because the probability of non-adiabatic transitions is abruptly enhanced when two energy levels approach each other [54], and it depends on many factors, including the relative phases in the wave function. This means that two slightly different initial conditions, with the same energy level populations, $|c_j|^2$, but different relative phases, behave in a totally different way at each avoided crossing. It is worth noting that the behavior would be totally different if the system were exactly integrable. In such a case, $[H, J'_z] = 0$, and all the transitions between energy levels with different quantum numbers $m' = \langle J'_z\rangle$ would be forbidden. Therefore, even though level crossings would become real under such circunstances, no transitions between the crossing levels would happen, and hence no changes in $\left\langle a^\dagger a\right\rangle_\infty$ (or any other observable) would be expected.

All these facts imply that slightly different initial conditions behave in a very different way at every avoided level crossing. Therefore we can conclude that *avoided crossings constitute an efficent mechanism of information erasing*. The microscopic differences in the relative phases of the wavefunction are amplified in these *critical* points, and they become visible in macroscopic equilibrium measurements, like $\left\langle a^\dagger a\right\rangle_\infty$ —each realization gives rise to a different value for $\left\langle a^\dagger a\right\rangle_\infty$. As a consequence, after the wavefunction goes through a few number of avoided crossings, it becomes very difficult to

trace back its past; equilibrium values, like $\left\langle a^{\dagger}a\right\rangle_{\infty}$, do not provide enough information. In other words, *our results show that avoided crossings enhance the sensitivity to initial conditions and contribute to rule out the fine details of the initial condition.*

These results provide a common scenario accounting for the adiabatic behavior, shown in Figs. 4 and 5, and real protocols with finite rapidity, displayed in Figs. 9 and 10. Avoided level crossings contribute to *hide* the information about the initial condition that remain stored during the whole protocol. Even though non-adiabatic transitions do not occur in the adiabatic limit, and therefore the distribution of coefficents $|c_j|^2$ remains unchanged, the swapping of the properties of anti-crossing eigenstates at every avoided level crossing imply that instantaneous eigenstates with different values of $\langle E_n| J'_z |E_n\rangle$ become populated, and, as a consequence, the unchanged distribution of coefficents $|c_j|^2$ eventually provides a good sampling of the microcanonical shell, giving rise to $\gamma \sim 0$ in Eq. (21), and hence making equilibrium states compatible with the standard microcanonical ensemble. At the same time, the very same avoided level crossings enhance the probability of non-adiabatic transitions if the protocol is performed at finite rapidity, and they also increase the differences between slightly different initial conditions, like the ones used in Fig. 10. This means that, if the protocol is not very slow, the information about the initial state is erased as soon as the system goes through a number of avoided level crossings, so that all the levels within the microcanonical shell become populated. If the protocol is much slower, this mechanism of information erasure does not act, but the same avoided level crossings contribute to hide the information stored in the coefficents $|c_j|^2$, from equilibrium measurements. We note here that non-equilibrium fluctuations relations might be sensitive to this information [46, 55].

Two remarks are important at this point. First, whereas the classical butterfly effect always occurs, the consequences of avoiding crossings are only relevant if the process is fast enough: all the non-adiabatic transitions can be removed if the characteristic time of the process is sufficently large [54]. This is what we observe in Fig. 9: the larger the characteristic time, the less efficient the information erasing mechanism is. Second, results in Fig. 10 show that this mechanism acts mainly nearby the integrable region, in contrast to the classical butterfly effect, which happens within the highly chaotic region. Therefore, it seems not linked to the quantum butterfly effect [56], which has been also found in the Dicke model [39]. We conjecture that this is a generic feature. As we have pointed out above, an exact integrable system has real crossings, due to the exact conservation rules [42, 43], but passing through them does not entail relevant consequences because of the very same conservation rules. However, as soon as integrability is broken, these conservation rules do not hold anymore, exact crossings become avoided crossings, and all non-adiabatic transitions become allowed. Hence, the information erasing mechanism is switched on as soon as integrability is broken. We note here that eigenstate deformations, giving rise to such avoided level crossings, have been recently proposed as a very senistive probe for the onset of quantum chaos [57]. Notwithstanding, it is also worth remarking that avoided level crossings, and therefore non-adiabatic transitions, also play a very relevant role within the highly chaotic region.

However, their consequences in the expected values of observables are less important, as we can see in panel (b) of Fig. 10: for $\lambda < 1.4$, $\sigma_{\langle a^\dagger a \rangle}$ is clearly smaller than for larger values of λ. We can infer an explanation from the results shown in Fig. 7. This figure focus on the expected values of J'_z in the eigenstates of the system at several values of λ, but a very similar picture is obtained if one works with $\left\langle a^\dagger a \right\rangle$ instead. In an almost integrable region, the regular structure shown in Peres lattices entails abrupt changes when non-adiabatic transitions take place, because they imply jumps from one line, characterized by certain values of the physical observables, to a different one, characterized by totally different values of the same physical observables (see, for example, panels (a) and (b) of Fig. 7). On the contrary, the same non-adiabatic transitions have almost no observable consequences in a highly chaotic region. As it is shown in panel (d) of Fig. 7 and it is stated in the ETH, neighboring eigenstates give rise to almost the same values of $\langle E_n | \mathcal{O} | E_n \rangle$, being $\mathcal{O}$ any physical observable, and therefore equilibrium expected values $\langle \mathcal{O} \rangle$ are not sensitive to non-adiabatic transitions. Therefore, we can conclue that the information erasing mechanism also takes place in highly chaotic region, even though it is much easier to detect when integrability is slightly broken. Finally, it is worth noting that, the larger the system size, the larger the number of avoided crossings, and therefore the more efficent information erasing mechanism, as it is shown in panel (b) of Fig. 9 That is, our results suggest that it is possible to prepare a state like $|\psi_2\rangle$ in small quantum systems, but becomes almost impossible if the system is large. More research is needed to explore the consequences of shortcuts to adiabaticity [58].

5. Discussion

Let us imagine that we obtain an equilibrium state like the ones displayed in Fig. 1, as the result of a simulation or an experiment. Our first, naïve, impression is that it is just an equilibrium state, storing no other information than its energy (or temperature). We have shown in this work that it may not be the case, if we are dealing with a not-so-large quantum system. An adiabatic protocol towards an integrable region can reveal a hidden piece of information stored in it. This means that, even though it looks like a perfectly thermalized state, only a specific subset of its eigenstates is populated. That is, this equilibrium state is really closer to the GGE than to the standard canonical or microcanonical ensembles, although it lays within a highly chaotic region. The eigenstate thermalization hypothesis, the mechanism explaining thermalization in isolated quantum systems, entails that this fact bears no consequences in the equilibrium values of physical observables, but non-equilibrium processes might not be oblivious to it and might give rise to anomalous work statistics [46, 55].

We have also shown that an efficent information erasing mechanism takes place if one parameter of the Hamiltonian is changed, and that the efficency of this mechanism is increased with the number of particles. This implies that, under realistic experimental conditions, it is very difficult to reproduce this result —except in quite small quantum

systems. This mechanism is linked to avoided level crossings, and is switched on as soon as integrability is broken. It implies that slightly different initial conditions give rise to different expected values of physical observables, specially when the system lays within an approximate integrable region, and therefore the ETH does not hold. A remarkable fact is that this very same phenomenon contributes to blur the consequences of reaching the adiabatic limit, in which this mechanism of information erasure does not hold.

These results uncover the differences between classical and quantum thermalization in isolated systems. In both cases, chaos plays a relevant role, implying equilibrium values of physical observables to be well described by means of the microcanonical ensemble, for which the (macroscopic) energy is the only relevant parameter. However, a relevant amount of information may still be present in quantum thermalized states, especially if the system is not very large. By contrast, classical thermalization always implies the erasure of such information.

Acknowledgments

This work has been supported by the Spanish Grant No. PGC2018-094180-B-I00 (MCIU/AEI/FEDER, EU). A. R. acknowledges A. L. Corps for his critical review of the manuscript.

References

[1] Reimann P 2008 Foundations of statistical mechanics under experimentally realistic conditions *Phys. Rev. Lett.* **101** 190403.
[2] Linden N, Popescu S, Short A J and Winter A 2009 Quantum mechanical evolution towards thermal equilibrium *Phys. Rev.* E **79** 061103.
[3] Srednicki M 1994 Chaos and quantum thermalization *Phys. Rev.* E **50** 888.
[4] Polkovnikov A, Sengputa K, Silva A and Vengalattore M 2011 Colloquium: Nonequilibrium dynamics of closed interacting quantum systems *Rev. Mod. Phys.* **83** 863.
[5] Jensen R V and Shankar R 1985 Statistical Behavior in Deterministic Quantum Systems with Few Degrees of Freedom *Phys. Rev. Lett.* **54** 1879.
[6] Deutsch J M 1991 Quantum statistical mechanics in a closed system *Phys. Rev.* A **43** 2046.
[7] Tasaki H 1998 From Quantum Dynamics to the Canonical Distribution: General Picture and a Rigorous Example *Phys. Rev. Lett.* **80** 1373.
[8] Rigol M, Dunjko V and Olshanii M 2008 Thermalization and its mechanism for generic isolated quantum systems *Nature* **452** 854.
[9] Reimann P 2015 Eigenstate thermalization: Deutsch's approach and beyond *New. J. Phys.* **17** 055025.
[10] Reimann P 2018 Dynamical typicality approach to eigenstate thermalization *Phys. Rev. Lett.* **120** 230601.
[11] Hamazaki R and Ueda M 2018 Atypicality of most few-body observables *Phys. Rev. Lett.* **120** 080603.
[12] Corps A L, Molina R A and Relaño A 2020 Thouless Energy Challenges Thermalization on the Ergodic Side of the Many-Body Localization Transition *Phys. Rev.* B **102** 014201.
[13] Corps A L, Molina R A and Relaño A 2021 Signatures of a critical point in the many-body localization transition, arXiv:2010.08759.

[14] Rigol M and Srednicki M 2012 Alternatives to Eigenstate Thermalization *Phys. Rev. Lett.* **108** 110601.
[15] Yan B and Sinitsyn N A 2020 Recovery of Damaged Information and the Out-of-Time-Ordered Correlators *Phys. Rev. Lett.* **125** 040605.
[16] Cao X and Scaffidi T 2021 Origin and limit of the recovery of damaged information by time reversal *Phys. Rev. A* **103** L020401.
[17] Dicke R H 1954 Coherence in Spontaneous Radiation Processes *Phys. Rev.* **93** 99.
[18] Baumann K, Guerlin C, Brennecke F and Esslinger T 2010 Dicke quantum phase transition with a superfluid gas in an optical cavity *Nature* **464** 1301.
[19] Baumann K, Mottl R, Brennecke F and Esslinger T 2011 Exploring Symmetry Breaking at the Dicke Quantum Phase Transition *Phys. Rev. Lett.* **107** 140402.
[20] Baden M P, Arnold K J, Grimsmo A L, Parkins S and Barrett M D 2017 Realization of the Dicke Model Using Cavity-Assisted Raman Transitions *Phys. Rev. Lett.* **113** 020408.
[21] Hamner C, Qu C, Zhang Y, Chang J, Gong M, Zhang C and Engels P 2014 Dicke-type phase transition in a spin-orbit-coupled Bose–Einstein condensate *Nat. Comms.* **5** 4023.
[22] Safavi-Naini A, Lewis-Swan R J, Bohnet J G, 3 Gärttner M, Gilmore K A, Jordan J E, Cohn J, Freericks J K, Rey A M and Bollinger J J 2018 Verification of a many-ion simulator of the Dicke model through slow quenches across a phase transition, Phys. Rev. Lett. **121** 040503.
[23] Lewis-Swan R J, Safavi-Naini A, Bollinger J J and Rey A M 2019 Unifying scrambling, thermalization and entanglement through measurement of fidelity out-of-time-order correlators in the Dicke model, Nat. Comm. **10**, 1581.
[24] Wang Y K and Hioe F T 1973 Phase Transition in the Dicke model of Superradiance *Phys. Rev. A* **7** 831.
[25] Hepp K and Lieb E H 1973 On the superradiant phase transition for molecules in a quantized radiation field: the dicke maser model *Ann. Phys. (N. Y.)* **76** 360.
[26] Hepp K and Lieb E H 1973 Equilibrium Statistical Mechanics of Matter Interacting with the Quantized Radiation Field *Phys. Rev. A* **8** 2517.
[27] Emary C and Brandes T 2003 Quantum Chaos Triggered by Precursors of a Quantum Phase Transition: The Dicke Model *Phys. Rev. Lett.* **90** 044101.
[28] Emary C and Brandes T 2003 Chaos and the quantum phase transition in the Dicke model *Phys. Rev. E* **67** 066203.
[29] Pérez-Fernández P, Relaño A, Arias J M, Cejnar P, Dukelsky J and García-Ramos J E 2011 Excited-state phase transition and onset of chaos in quantum optical models *Phys. Rev.* E **83** 046208.
[30] Puebla R, Relaño A and Retamosa J 2013 Excited-state phase transition leading to symmetry-breaking steady states in the Dicke model *Phys. Rev.* A **87**, 023819 (2013).
[31] Brandes T 2013 Excited-state quantum phase transitions in Dicke superradiance models *Phys. Rev.* E **88** 032133.
[32] Bastarrachea-Magnani M A, Lerma-Hernández S and Hirsch JG 2014 Comparative quantum and semiclassical analysis of atom-field systems. I. Density of states and excited-state quantum phase transitions *Phys. Rev.* A **89** 032101.
[33] Relaño A, Bastarrachea-Magnani M A and Lerma-Hernández S 2016 Approximated integrability of the Dicke model *EPL* **116** 50005.
[34] Bastarrachea-Magnani M A, Relaño A, Lerma-Hernández S, López-del-Carpio L, Chávez-Carlos J and Hirsch J G 2017 Adiabatic invariants for the regular region of the Dicke model *J. Phys.* A **50** 144002.
[35] Bastarrachea-Magnani M A, Lerma-Hernández S and Hirsch JG 2014 Comparative quantum and semiclassical analysis of atom-field systems. II. Chaos and regularity *Phys. Rev.* A **89** 032102.
[36] Chávez-Carlos J, Bastarrachea-Magnani M A, Lerma-Hernández S and Hirsch J G 2016 Classical chaos in atom-field systems *Phys. Rev.* E **94** 022209.
[37] Villasenor D, Pilatowsky-Cameo S, Bastarrachea-Magnani M A, Lerma-Hernández S, Santos L

F and Hirsch J G 2020 Quantum vs classical dynamics in a spin-boson system: manifestations of spectral correlations and scarring *New. J. Phys.* **22** 063036.

[38] Ribeiro A D, de Aguiar M A M and de Toledo Piza A F R 2006 The semiclassical coherent state propagator for system with spin *J. Phys.* A **39** 3085.

[39] Chávez-Carlos J, López-del-Carpio B, Bastarrachea-Magnani M A, Stránský P, Lerma-Hernández S, Santos L F and Hirsch J G 2019 Quantum and Classical Lyapunov Exponents in Atom-Field Interaction Systems *Phys. Rev. Lett.* **122** 024101.

[40] Pilatowsky-Cameo S, Chávez-Carlos J, Bastarrachea-Magnani M A, Stránský P, Lerma-Hernández S, Santos L F and Hirsch J G 2020 Positive quantum Lyapunov exponents in experimental systems with a regular classical limit *Phys. Rev. E* **101** 010202.

[41] Albash T and Lidar D A 2018 Adiabatic quantum computing *Rev. Mod. Phys.* **90** 015002.

[42] Yuzbashyan E A, Altshuler B L and Shastry B S 2002 The origin of degeneracies and crossings in the 1d Hubbard model *J. Phys.* A **35** 7525.

[43] Owusu H K, Wagh K and Yuzbashyan E A 2009 The link between integrability, level crossings and exact solutions in quantum models *J. Phys.* A **42** 035206.

[44] Berry M V 1984 Quantal Phase Factors Accompanying Adiabatic Changes *Proc. Roy. Soc.* A **392** 1802.

[45] Puebla R and Relaño A 2015 Irreversible processes without energy dissipation in an isolated Lipkin-Meshkov-Glick model *Phys. Rev.* E **92** 012101.

[46] Mur-Petit J, Relaño A, Molina R A and Jaksch D 2018 Revealing missing charges with generalised quantum fluctuation relations *Nat. Comm.* **9** 2006.

[47] Lóbez C M and Relaño A 2016 Entropy, chaos and excited-state quantum phase transitions in the Dicke model *Phys. Rev.* E **94** 042140.

[48] Rigol M, Dunjko V, Yurovsky V and Olshanii M 2007 Relaxation in a completely integrable manybody quantum system: An ab initio study of the dynamics of the highly excited states of 1D lattice hard-core bosons *Phys. Rev. Lett.* **98** 050405.

[49] Cassidy A C, Clark C W and Rigol M 2011 Generalized thermalization in an integrable lattice system *Phys. Rev. Lett.* **106** 140405.

[50] Jaynes E T 1957 Information theory and statistical mechanics *Phys. Rev.* **106** 620.

[51] Jaynes E T 1957 Information theory and statistical mechanics. II *Phys. Rev.* **108** 171.

[52] Relaño A 2010 Thermalization in an interacting spin system in the transition from integrability to chaos *J. Stat. Mech.* P07016.

[53] Peres A 1984 New Conserved Quantities and Test for Regular Spectra *Phys. Rev. Lett.* **53** 1711.

[54] Landau L 1932 Zur theorie der Energieubertragung I *Physikalische Zeitschrift der Sowjetunion* **2** 46; Zener C 1932 Non-adiabatic crossing of energy levels *Proc. Roc. Soc. Lond.* A **137** 696.

[55] Relaño A 2018 Anomalous Thermalization in Quantum Collective Models *Phys. Rev. Lett.* **121** 030602.

[56] Maldacena J, Shenker S H and Stanford D 2016 A bound on chaos *J. High Energy Phys.* **08** 106.

[57] Pandey M, Claeys P W, Campbell D K, Polkovnikov A and Sels D 2020 Adiabatic eigenstate deformation as a sensitive probe for quantum chaos *Phys. Rev.* X **10** 041017.

[58] Guéry-Odelin D, Ruschhaupt A, Kiely A, Torrontegui E, Martínez-Garaot S and Muga J G 2019, Shortcuts to adiabaticity: Concepts, methods, and applications *Rev. Mod. Phys.* **91** 045001.